particles

MDPI

Review

Probes of Lepton Flavor Universality in $b \to u$ Transitions

Pietro Colangelo [1,*], Fulvia De Fazio [1] and Francesco Loparco [1,2]

[1] Istituto Nazionale di Fisica Nucleare - Sezione di Bari, via Orabona 4, 70126 Bari, Italy; fulvia.defazio@ba.infn.it (F.D.F.); Francesco.Loparco1@ba.infn.it (F.L.)

[2] Dipartimento Interateneo di Fisica "M. Merlin" dell'Universitá e Politecnico di Bari, via Orabona 4, 70126 Bari, Italy

* Correspondence: pietro.colangelo@ba.infn.it

Received: 7 January 2020; Accepted: 17 February 2020; Published: 27 February 2020

Abstract: Anomalies recently observed in semileptonic $b \to c\ell^-\bar{\nu}_\ell$ and $b \to s\ell^+\ell^-$ transitions point to violation of Lepton Flavour Universality. Strategies for new analyses of different modes are required, in particular for the modes induced by the $b \to u$ transition. We describe the purely leptonic B decay, the $\bar{B} \to \pi\ell^-\bar{\nu}_\ell$ channel and the B semileptonic modes to $\rho(770)$ and $a_1(1260)$ in extensions of the Standard Model involving Lepton Flavour Universality violating $b \to u$ operators. In particular, we review the observables in the four-dimensional angular $\bar{B} \to \rho(\pi\pi)\ell^-\bar{\nu}_\ell$ and $\bar{B} \to a_1(\rho\pi)\ell^-\bar{\nu}_\ell$ distributions, suitable to pin down deviations from the Standard Model. We discuss the complementarity among the various modes for New Physics searches.

Keywords: Lepton Flavour Universality; semileptonic B decays

1. Introduction

Several anomalies have recently emerged in tree-level $b \to c\ell^-\bar{\nu}_\ell$ and in loop-induced $b \to s\ell^+\ell^-$ semileptonic transitions. In tree-level modes, the measured ratios $R(D^{(*)}) = \dfrac{\mathcal{B}(B \to D^{(*)}\tau^-\bar{\nu}_\tau)}{\mathcal{B}(B \to D^{(*)}\ell^-\bar{\nu}_\ell)}$ (with $\ell = e, \mu$) [1–9] exceed the Standard Model (SM) predictions at $3.1\,\sigma$ [10]. This is remarkable, since the hadronic uncertainties largely cancel out in the ratios [11,12]. The measurement of $R(J/\psi) = \dfrac{\mathcal{B}(B_c^+ \to J/\psi\tau^+\nu_\tau)}{\mathcal{B}(B_c^+ \to J/\psi\mu^+\nu_\mu)}$ [13] is also above the (more uncertain) SM expectation [14–17]. For neutral current $b \to s$ semileptonic modes, the ratios $R_{K^{(*)}} = \dfrac{\int_{q^2_{min}}^{q^2_{max}} \frac{d\Gamma}{dq^2}(B^+ \to K^{(*)}\mu^+\mu^-)dq^2}{\int_{q^2_{min}}^{q^2_{max}} \frac{d\Gamma}{dq^2}(B^+ \to K^{(*)}e^+e^-)dq^2}$, measured in various ranges of the q^2 dilepton invariant mass [18–20], also deviate from the SM predictions, which are close to one. Tests involving Λ_b decay modes are also carried out [21]. The anomalies point to violation of lepton flavour universality (LFU), which is an accidental SM symmetry, broken by the Yukawa interactions (a review is in Reference [22]).

There are other tensions, namely the difference in the value of $|V_{cb}|$, an element of the Cabibbo-Kobayashi-Maskawa quark mixing matrix, when determined using inclusive $\bar{B} \to X_c\ell^-\bar{\nu}_\ell$ observables (width and moments) and exclusive modes, mainly $\bar{B} \to D^*\ell^-\bar{\nu}_\ell$. The tension persists after recent experimental analyses [23,24]. The latest measurement using $B_s^0 \to D_s^{(*)-}\mu^+\nu_\mu$ agrees with the inclusive determination, but it is affected by a sizable error [25]. Even though its solution within SM is possible [26–29], a connection with the $b \to c$ semileptonic anomalies can also be envisaged in frameworks incorporating LFU violation [12,30]. Experimental signatures of Beyond

the Standard Model (BSM) effects in such modes have been scrutinized, in particular using the full $\bar{B} \to D^*(D\pi, D\gamma)\ell^-\bar{\nu}_\ell$ decay distributions for different lepton species [31–35].

Although the semileptonic $b \to u$ transitions are CKM suppressed with respect to the $b \to c$ ones, new precision measurements are foreseen by LHCb and Belle II Collaborations. At present, there is a tension between the inclusive determination of $|V_{ub}|$ and the exclusive measurement from the $\bar{B} \to \pi\ell^-\bar{\nu}_\ell$ decay width. The B^- purely leptonic and the semileptonic $B \to \pi$ mode have been analyzed in References [36–43], showing their sensitivity to BSM effects. Other decay modes can be exploited to pin down possible deviation from the Standard Model, in particular those involving several hadrons in the final state. This is the case of B to vector $\rho(770)$ and axial-vector $a_1(1260)$ channels, for which the fully differential angular distributions, when ρ decays in two pions and a_1 decays into $\rho\pi$, produce a wealth of correlated observables, with coherent patterns within and beyond SM.

We extend the semileptonic $b \to u$ effective Hamiltonian with the inclusion of additional scalar (S), pseudoscalar (P), vector (V) and tensor (T) operators, and study the effects of such operators on $\bar{B}$ transitions to leptons and to $\pi\ell\bar{\nu}$. Then, we provide the expressions of the fully differential decay distributions for the $\bar{B} \to \rho(\pi\pi)\ell^-\bar{\nu}_\ell$ and $\bar{B} \to a_1(\rho\pi)\ell^-\bar{\nu}_\ell$ modes (Section 4). In the Large Energy Limit for the light mesons, the distributions are expressed in terms of a small number of hadronic form factors. Observables in $\bar{B} \to \rho(\pi\pi)\ell^-\bar{\nu}_\ell$ are studied at a benchmark point in the parameter space of the new effective couplings, scrutinizing their sensitivity to the different operators (Section 5). For the $a_1(1260)$ mode, analyzed in Section 6, the uncertainties from the form factors are large; nevertheless, also in this channel observables particularly sensitive to New Physics (NP) can be identified [44].

2. Extended $b \to u\ell^-\bar{\nu}_\ell$ Effective Hamiltonian

Beyond the Standard Model (BSM) effects in beauty hadron decays can be analyzed using the Standard Model Effective Field Theory. For a NP scale Λ_{NP} much larger than the EW scale the new massive degrees of freedom can be integrated out, recovering an effective Hamiltonian involving SM fields and invariant under the SM gauge group. This Hamiltonian contains additional operators with respect to SM, suppressed by powers of Λ_{NP}: dimension-six four-fermion operators appear at $\mathcal{O}\left(1/\Lambda_{NP}^2\right)$ [45]. We consider the general expression of the effective $b \to u$ Hamiltonian:

$$\begin{aligned} H_{\text{eff}}^{b\to u\ell\nu} &= \frac{G_F}{\sqrt{2}} V_{ub} \Big\{ (1+\epsilon_V^\ell)\, (\bar{u}\gamma_\mu(1-\gamma_5)b)\, (\bar{\ell}\gamma^\mu(1-\gamma_5)\nu_\ell) + \epsilon_S^\ell\, (\bar{u}b)\, (\bar{\ell}(1-\gamma_5)\nu_\ell) \\ &+ \epsilon_P^\ell\, (\bar{u}\gamma_5 b)\, (\bar{\ell}(1-\gamma_5)\nu_\ell) + \epsilon_T^\ell\, (\bar{u}\sigma_{\mu\nu}(1-\gamma_5)b)\, (\bar{\ell}\sigma^{\mu\nu}(1-\gamma_5)\nu_\ell) \Big\} + h.c., \end{aligned} \tag{1}$$

consisting in the SM term and in NP operators with complex lepton-flavour dependent couplings $\epsilon_{V,S,P,T}^\ell$. V_{ub} and ϵ_V^ℓ are independent parameters. A purely left-handed lepton current is assumed. Moreover, the quark right-handed vector current is excluded, since the only four-fermion operator of this type, invariant under the SM group, is non-linear in the Higgs field [46–48]. See References [37,38,40] for investigations of right-handed currents. The Hamiltonian (1) governs decays of B mesons, of B_s (such as $B_s \to K^{(*)+}\ell^-\bar{\nu}_\ell$), B_c (e.g., $B_c \to D^{(*)+}\ell^-\bar{\nu}_\ell$ [49]), Λ_b (e.g., $\Lambda_b \to p\ell^-\bar{\nu}_\ell$ [50]), and so forth. Here we focus on B meson modes, for which precise measurements are available.

3. $B^- \to \ell^-\bar{\nu}_\ell$ and $\bar{B} \to \pi\ell^-\bar{\nu}_\ell$

The couplings of the NP operators in (1) are constrained by the purely leptonic B^- and semileptonic $\bar{B} \to \pi\ell^-\bar{\nu}_\ell$ modes. The $B^- \to \ell^-\bar{\nu}_\ell$ decay width obtained from Equation (1),

$$\Gamma(B^- \to \ell^-\bar{\nu}_\ell) = \frac{G_F^2 |V_{ub}|^2 f_B^2 m_B^3}{8\pi} \left(1 - \frac{m_\ell^2}{m_B^2}\right)^2 \left| \left(\frac{m_\ell}{m_B}\right)(1+\epsilon_V^\ell) + \frac{m_B}{m_b+m_u}\epsilon_P^\ell \right|^2, \tag{2}$$

with f_B defined as $\langle 0|\bar{u}\gamma_\mu\gamma_5 b|\bar{B}(p)\rangle = i f_B p_\mu$, shows that this mode is insensitive to the scalar and tensor operators. The pseudoscalar operator lifts the helicity suppression, which is effective for light leptons. This produces stringent bounds to $\epsilon_P^{e,\mu}$.

The $\bar{B} \to \pi\ell^-\bar{\nu}_\ell$ decay distribution in the dilepton mass squared q^2, obtained using (1) and adopting the definition of the form factors $f_i(q^2) = f_i^{B\to\pi}(q^2)$ as in Reference [44],

$$\begin{aligned}\frac{d\Gamma}{dq^2}(\bar{B}\to\pi\ell^-\bar{\nu}_\ell) &= \frac{G_F^2|V_{ub}|^2\lambda^{1/2}(m_B^2,m_\pi^2,q^2)}{128 m_B^3\pi^3 q^2}\left(1-\frac{m_\ell^2}{q^2}\right)^2 \\ &\times \left\{\left|m_\ell(1+\epsilon_V^\ell)+\frac{q^2\epsilon_S^\ell}{m_b-m_u}\right|^2 (m_B^2-m_\pi^2)^2 f_0^2(q^2)+\right. \\ &+ \lambda(m_B^2,m_\pi^2,q^2)\left[\frac{1}{3}\left|m_\ell(1+\epsilon_V^\ell)f_+(q^2)+\frac{4q^2}{m_B+m_\pi}\epsilon_T^\ell f_T(q^2)\right|^2\right. \\ &+ \left.\left.\frac{2q^2}{3}\left|(1+\epsilon_V^\ell)f_+(q^2)+4\frac{m_\ell}{m_B+m_\pi}\epsilon_T^\ell f_T(q^2)\right|^2\right]\right\}, \end{aligned} \tag{3}$$

(with λ the triangular function), shows that the operator P does not contribute in this case. In Equations (2) and (3) the CKM matrix element V_{ub} appears in the combination $V_{ub}(1+\epsilon_V^\ell)$. The lepton-flavour dependence of the effective couplings ϵ_V^ℓ would produce different values of an effective $|V_{ub}|$ when measured in channels involving different lepton generations.

In the B rest-frame the energy E of the emitted pion is obtained by the relation $q^2 = m_B^2 + m_\pi^2 - 2m_B E$, and is in the range $m_\pi \le E \le \frac{m_B}{2}\left(1+\frac{m_\pi^2}{m_B^2}-\frac{m_\ell^2}{m_B^2}\right)$. In the Large Energy Limit, $E \simeq \frac{m_B}{2}$, the $\bar{B}\to\pi\ell^-\bar{\nu}$ distribution involves a single form factor ξ_π [51,52]. The consequence is that, in this limit, the ratios

$$\frac{dR(\pi)^{\ell\ell'}}{dE} = \frac{d\Gamma}{dE}(\bar{B}\to\pi\ell^-\bar{\nu}_\ell)/\frac{d\Gamma}{dE}(\bar{B}\to\pi\ell'^-\bar{\nu}_{\ell'}) \tag{4}$$

are free of hadronic uncertainties and only involve combinations of $\epsilon_{V,S,T}^{\ell,\ell'}$ [44] .

4. $\bar{B}\to\rho(\to\pi\pi)\ell^-\bar{\nu}_\ell$ and $\bar{B}\to a_1(\to\rho\pi)\ell^-\bar{\nu}_\ell$ Full Angular Distributions

For the modes $\bar{B}\to\rho(\to\pi\pi)\ell^-\bar{\nu}_\ell$ and $\bar{B}\to a_1(\to\rho\pi)\ell^-\bar{\nu}_\ell$, the main sensitivity to the new operators in (1) is in the 4-dimensional differential decay distribution in (q^2, θ, θ_V, ϕ), with angles defined in Figure 1.

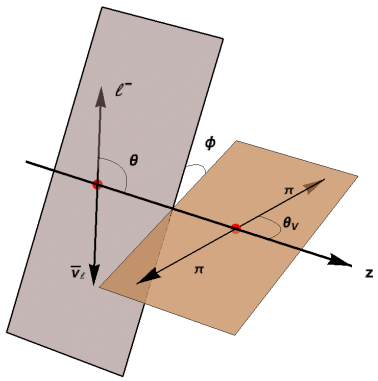

Figure 1. Definition of the angles in the fully differential $\bar{B}\to\rho(\pi\pi)\ell^-\bar{\nu}_\ell$ distribution. The $\rho\to\pi\pi$ and $W^-\to\ell^-\bar{\nu}_\ell$ decay planes are shown.

For the ρ mode the distribution reads:

$$\begin{aligned}\frac{d^4\Gamma(\bar{B}\to\rho(\to\pi\pi)\ell^-\bar{\nu}_\ell)}{dq^2\,d\cos\theta\,d\phi\,d\cos\theta_V} &= \mathcal{N}_\rho|\vec{p}_\rho|\left(1-\frac{m_\ell^2}{q^2}\right)^2\Big\{I_{1s}^\rho\,\sin^2\theta_V+I_{1c}^\rho\,\cos^2\theta_V\\ &+\left(I_{2s}^\rho\,\sin^2\theta_V+I_{2c}^\rho\,\cos^2\theta_V\right)\cos 2\theta\\ &+I_3^\rho\,\sin^2\theta_V\sin^2\theta\cos 2\phi+I_4^\rho\,\sin 2\theta_V\sin 2\theta\cos\phi\\ &+I_5^\rho\,\sin 2\theta_V\sin\theta\cos\phi+\left(I_{6s}^\rho\,\sin^2\theta_V+I_{6c}^\rho\,\cos^2\theta_V\right)\cos\theta\\ &+I_7^\rho\,\sin 2\theta_V\sin\theta\sin\phi\Big\}\,,\end{aligned}\tag{5}$$

with $\mathcal{N}_\rho=\dfrac{3G_F^2|V_{ub}|^2\mathcal{B}(\rho\to\pi\pi)}{128(2\pi)^4m_B^2}$. Other angular structures appear in the differential distribution if the quark right-handed vector operator is included in (1). The same expression holds for $B_s\to K^{*+}(K\pi)\ell^-\bar{\nu}_\ell$. The relations of the angular coefficient functions in Equation (5) to the hadronic $B\to\rho$ matrix elements are collected in Reference [44], obtained in the narrow width approximation which factorizes the production and decay amplitude of the intermediate vector meson. A discussion on this procedure, together with references to studies of non-resonant contributions, can also be found in Reference [44].

For the $a_1(\rho\pi)$ channel with the final ρ transversely ($\rho_\perp$) or longitudinally ($\rho_\parallel$) polarized, the 4-dimensional distribution has the same expression as in (5) with the substitution $I_i^\rho\to I_{i,\parallel,\perp}^{a_1}$ and $\mathcal{N}_\rho\to\mathcal{N}_{a_1}^{\parallel(\perp)}=\dfrac{3G_F^2|V_{ub}|^2\mathcal{B}(a_1\to\rho_{\parallel(\perp)}\pi)}{128(2\pi)^4m_B^2}$. The subscripts $\perp$ and $\parallel$ refer to the ρ polarizations. The expressions of the coefficient functions in terms of $B\to a_1$ hadronic matrix elements are in Reference [44]. The separation of the polarizations of the final ρ is justified by the different sensitivity of the distribution to the NP operators.

The angular functions I_i^ρ (I_i^{a1}) in Equation (5) have the general expression

$$\begin{aligned}I_i &= |1+\epsilon_V|^2\,I_i^{SM}+|\epsilon_X|^2I_i^{NP,X}+|\epsilon_T|^2I_i^{NP,T}+2\,\mathrm{Re}\left[\epsilon_X(1+\epsilon_V^*)\right]I_i^{INT,X}\\ &+2\,\mathrm{Re}\left[\epsilon_T(1+\epsilon_V^*)\right]I_i^{INT,T}+2\,\mathrm{Re}\left[\epsilon_X\epsilon_T^*\right]I_i^{INT,XT},\qquad (i=1,\ldots 6),\\ I_7 &= 2\,\mathrm{Im}\left[\epsilon_X(1+\epsilon_V^*)\right]I_7^{INT,X}+2\,\mathrm{Im}\left[\epsilon_T(1+\epsilon_V^*)\right]I_7^{INT,T}+2\,\mathrm{Im}\left[\epsilon_X\epsilon_T^*\right]I_7^{INT,XT},\end{aligned}\tag{6}$$

with $X=P$ in case of ρ, and $X=S$ for a_1, and functions I_i^{SM}, I_i^{NP} and I_i^{INT} collected in Reference [44]. All angular coefficient functions, with the exception of I_7, do not vanish in SM and are sensitive to ϵ_V. Structures able to disentangle the other S, P and T operators can be identified. For $B\to\rho\ell\bar{\nu}_\ell$, the functions I_{1s}^ρ, I_{2s}^ρ, I_{2c}^ρ, I_3^ρ, I_4^ρ, I_{6s}^ρ do not depend on ϵ_P and are only sensitive to the tensor operator. The corresponding quantities in $B\to a_1(\rho_\parallel\pi)\ell\bar{\nu}_\ell$ do not depend on ϵ_S. In $B\to a_1(\rho_\perp\pi)\ell\bar{\nu}_\ell$ the functions $I_{1c,\perp}^{a_1}$, $I_{2s,\perp}^{a_1}$, $I_{2c,\perp}^{a_1}$, $I_{3,\perp}^{a_1}$, $I_{4,\perp}^{a_1}$, $I_{6c,\perp}^{a_1}$ are insensitive to the scalar operator. There are angular coefficient functions related only to the helicity amplitudes corresponding to the transversely polarized W, hence to transverse ρ (a_1) in $B\to\rho\ell\bar{\nu}_\ell$ ($B\to a_1\ell\bar{\nu}_\ell$). Such observables depend on ϵ_T, not on ϵ_P (in the ρ channel) or ϵ_S (in a_1).

In the Large Energy Limit of the light meson, the $B\to\rho(a_1)$ weak matrix elements can be written in terms of two form factors, $\xi_\perp^\rho(\xi_\perp^{a_1})$ and $\xi_\parallel^\rho(\xi_\parallel^{a_1})$ [44]. In this limit, several angular coefficients depend only on $\xi_\perp$, others involve both $\xi_\perp$ and $\xi_\parallel$. The coefficients depending only on $\xi_\perp^{\rho,a_1}(E)$ are, in $B\to\rho$, I_{1s}^ρ, I_{2s}^ρ, I_3^ρ and I_{6s}^ρ, and in $B\to a_1$ $I_{1s,\parallel}^{a_1}$, $I_{2s,\parallel}^{a_1}$, $I_{3,\parallel}^{a_1}$ and $I_{6s,\parallel}^{a_1}$ (for longitudinally polarized ρ), and $I_{1c,\perp}^{a_1}$, $I_{2c,\perp}^{a_1}$, $I_{3,\perp}^{a_1}$ and $I_{6c,\perp}^{a_1}$ (for transversely polarized ρ). When a single form factor is involved, ratios of coefficient functions are free of hadronic uncertainties.

5. Observables in $\bar{B} \to \rho(\pi\pi)\ell^-\bar{\nu}_\ell$

To give examples of the effects of NP operators in (1) in $\bar{B} \to \rho\ell^-\bar{\nu}_\ell$, we constrain the space of the effective couplings using a set of hadronic quantities and the available data. The couplings ϵ_V^μ, ϵ_P^μ, ϵ_T^μ are constrained by the measurements of $\mathcal{B}(\bar{B}^0 \to \pi^+\ell^-\bar{\nu}_\ell)$ and $\mathcal{B}(\bar{B}^0 \to \rho^+\ell^-\bar{\nu}_\ell)$ [53], together with $\mathcal{B}(B^- \to \mu^-\bar{\nu}_\mu)$ [54] and $\mathcal{B}(B^- \to e^-\bar{\nu}_e)$, $\mathcal{B}(B^- \to \tau^-\bar{\nu}_\tau)$ [53]. An upper bound $\mathcal{B}(\bar{B}^0 \to \pi^+\tau^-\bar{\nu}_\tau)$ has been established [55]. We use the $B \to \pi$ form factors in Appendix A and the $B \to \rho$ form factors in Reference [56]. The parameter space for the NP couplings, together with the chosen benchmark point, is shown in Figure 2 in the case of μ and τ. The $\bar{B} \to \pi\,\mu^-\,\bar{\nu}_\mu$ decay distribution, using the form factors in Appendix A, is depicted in Figure 3 for SM and NP at the benchmark point, compared to Belle [57] and BaBar measurements [58,59].

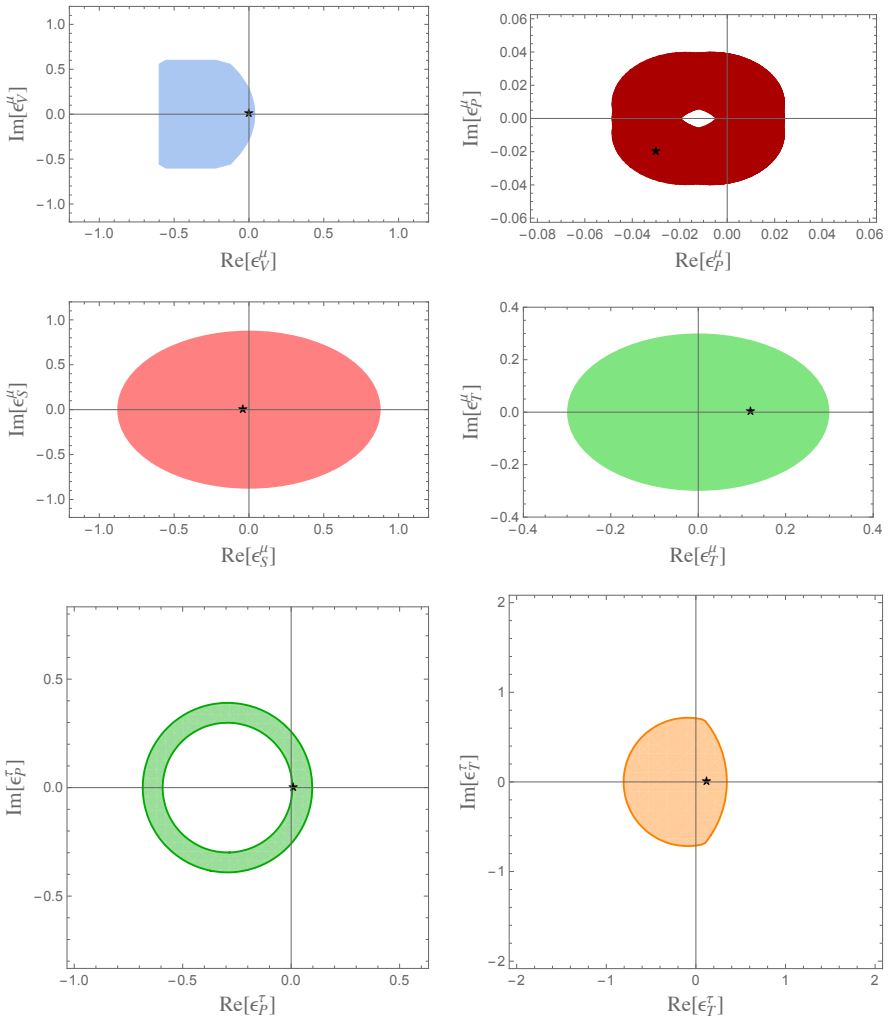

Figure 2. Allowed regions (at 68% CL) for the couplings ϵ_V^μ and ϵ_P^μ, (first row plots), ϵ_S^μ and ϵ_T^μ (second row plots). The stars are the benchmark points: $(\mathrm{Re}[\epsilon_V^\mu], \mathrm{Im}[\epsilon_V^\mu]) = (0, 0)$, $(\mathrm{Re}[\epsilon_P^\mu], \mathrm{Im}[\epsilon_P^\mu]) = (-0.03, -0.02)$, $(\mathrm{Re}[\epsilon_T^\mu], \mathrm{Im}[\epsilon_T^\mu]) = (0.12, 0)$ and $(\mathrm{Re}[\epsilon_S^\mu], \mathrm{Im}[\epsilon_S^\mu]) = (-0.04, 0)$, with $|V_{ub}| = 3.5 \times 10^{-3}$. The plots in the third row show the allowed regions for the couplings ϵ_P^τ and ϵ_T^τ, with the stars indicating the benchmark points $\epsilon_V^\tau = 0$, $\epsilon_S^\tau = 0$, $(\mathrm{Re}[\epsilon_P^\tau], \mathrm{Im}[\epsilon_P^\tau]) = (0.01, 0)$ and $(\mathrm{Re}[\epsilon_T^\tau], \mathrm{Im}[\epsilon_T^\tau]) = (0.12, 0)$. The various colors indicate the different couplings.

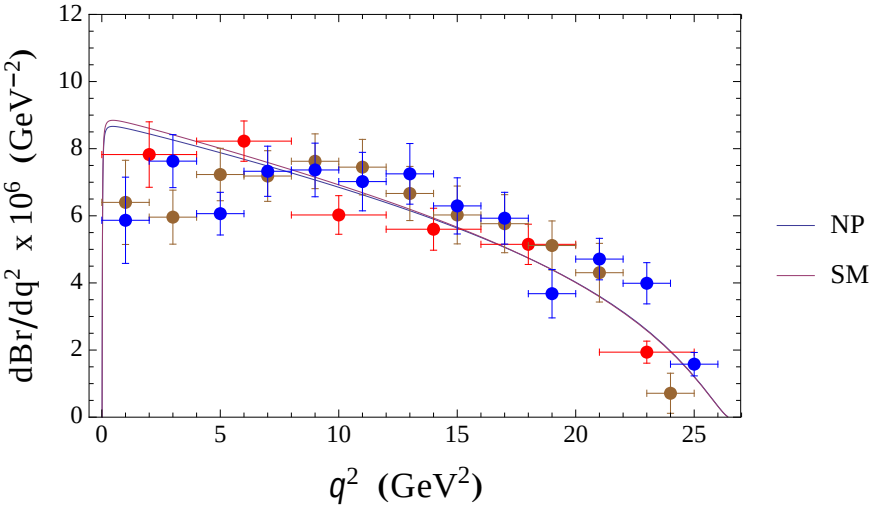

Figure 3. $\bar{B} \to \pi\,\mu^-\,\bar{\nu}_\mu$ distribution using the form factors in Appendix A and parameters in Table A1, in Standard Model (SM) and in New Physics (NP) at the benchmark point. The red and brown data are from Babar [58,59], the blue ones from Belle Collaboration [57].

The functions I^ρ_{1s}, I^ρ_{2s}, I^ρ_{2c}, I^ρ_3, I^ρ_4 and I^ρ_{6s}, which are independent of ϵ_P, are shown in Figure 4 for SM and NP. The bands are obtained varying the form factor parameters within their estimated ranges. Notice the zero in $I^\rho_{2s}(q^2)$, absent in SM.

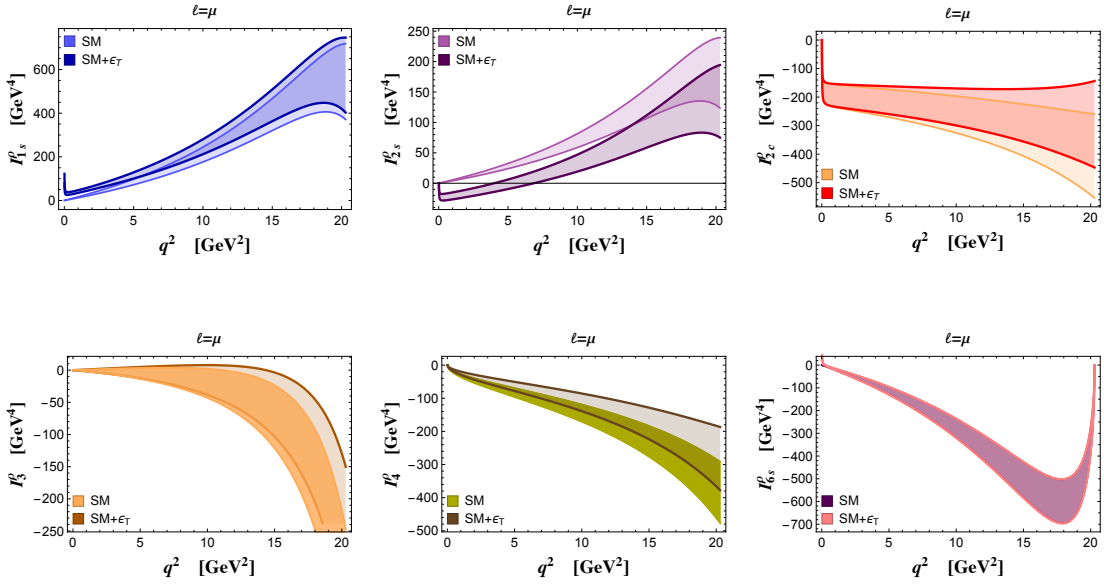

Figure 4. $\bar{B} \to \rho(\pi\pi)\,\mu^-\,\bar{\nu}_\mu$: angular coefficient functions $I^\rho_i(q^2)$ in Equation (5), for SM and NP at the benchmark point. The bands for SM and NP, with the colors indicated in each plot, are obtained varying the form factor parameters within the estimated ranges. A zero in $I^\rho_{2s}(q^2)$ appears in NP.

The other coefficient functions are in Figure 5, and there is a zero in $I^{\rho}_{6c}(q^2)$ not present in SM. The function I^{ρ}_{7} in Figure 6 vanishes in SM, and is only sensitive to the imaginary part of the NP couplings. For the τ modes, the angular functions are in Figures 7 and 8, and also for this mode I^{ρ}_{6c} has a zero in NP, not in SM.

Let us consider the ratios

$$R^{\rho}_{2s/1s}(q^2) = \frac{I^{\rho}_{2s}(q^2)}{I^{\rho}_{1s}(q^2)}, \tag{7}$$

$$R^{a_1,\parallel}_{2s/1s}(q^2) = \frac{I^{a_1}_{2s,\parallel}(q^2)}{I^{a_1}_{1s,\parallel}(q^2)}, \tag{8}$$

and $R^{a_1,\parallel}_{2s/1s} = R^{a_1,\perp}_{2c/1c}$. $R^{\rho}_{2s/1s}$ is form factor independent in SM. In NP it is still form factor independent in the Large Energy Limit, since I^{ρ}_{2s} and I^{ρ}_{1s} depend on $\xi^{\rho}_{\perp}$. As shown in Figure 9, the ratio (7) has a zero in NP, not in SM, whose position $q^2_{0,\rho}$ depends only on $|\epsilon^{\mu}_T|$ with a small form factor effect. In the Large Energy Limit we have

$$|\epsilon^{\mu}_T|^2 = \frac{q^2_{0,\rho}}{16 m_B^2} \frac{\lambda(m_B^2, m_\rho^2, q^2_{0,\rho}) + 2 m_B^2 m_\rho^2}{\lambda(m_B^2, m_\rho^2, q^2_{0,\rho}) + 2 q^2_{0,\rho} m_\rho^2}. \tag{9}$$

Analogously, for the $(a_1)_{\parallel}$ channel (for $(a_1)_{\perp}$ considering $R_{2c/1c}$) we have:

$$|\epsilon^{\mu}_T|^2 = \frac{q^2_{0,a_1}}{16 m_B^2} \frac{\lambda(m_B^2, m_{a_1}^2, q^2_{0,a_1}) + 2 m_B^2 m_{a_1}^2}{\lambda(m_B^2, m_{a_1}^2, q^2_{0,a_1}) + 2 q^2_{0,a_1} m_{a_1}^2}. \tag{10}$$

The positions of the zeros in two modes are related, and their measurement would provide access to the tensor operator.

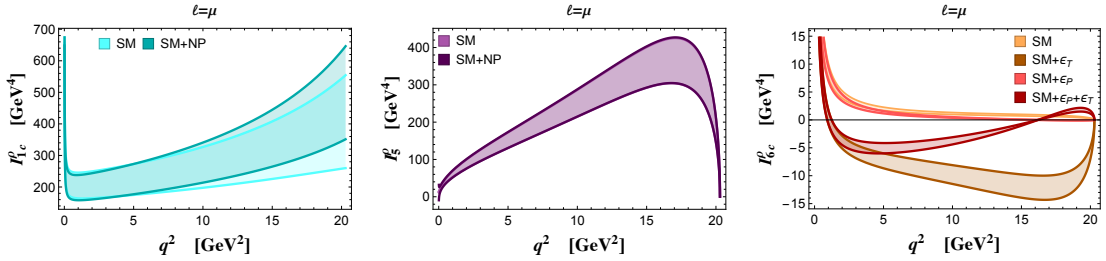

Figure 5. $\bar{B} \to \rho(\pi\pi)\, \mu^- \bar{\nu}_\mu$: angular coefficient functions $I^{\rho}_{1c}(q^2)$ (**left**), $I^{\rho}_{5}(q^2)$ (**middle**) and $I^{\rho}_{6c}(q^2)$ (**right**).

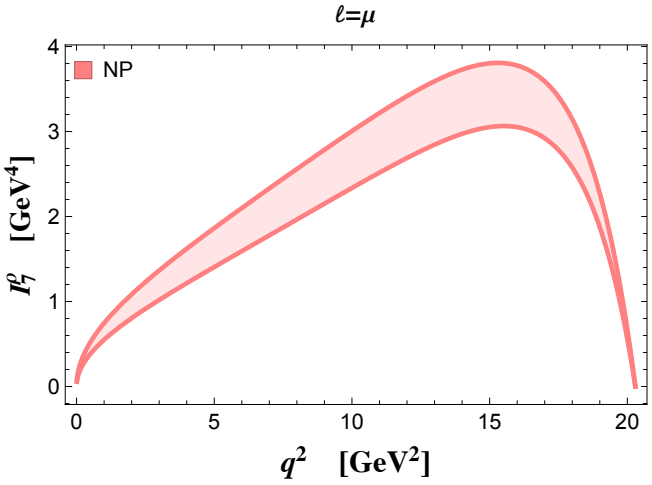

Figure 6. $\bar{B} \to \rho(\pi\pi)\,\mu^-\,\bar{\nu}_\mu$: angular coefficient function in NP at the benchmark point.

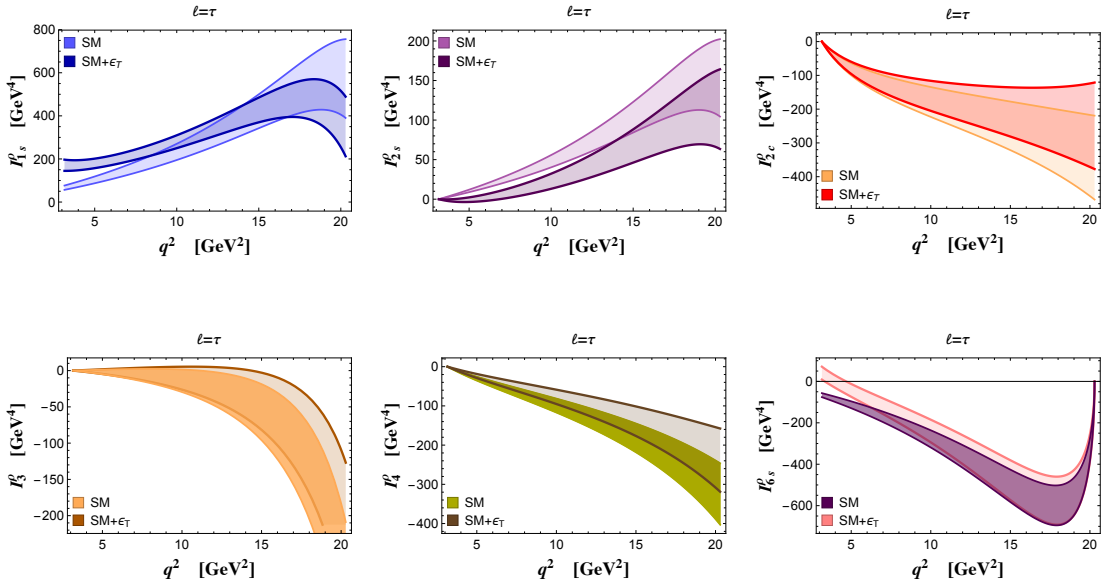

Figure 7. $\bar{B} \to \rho(\pi\pi)\,\tau^-\,\bar{\nu}_\tau$ mode: angular coefficient functions $I_i^\rho(q^2)$ in Equation (5). The bands for SM and NP, with colors indicated in each plot, are obtained varying the form factor parameters.

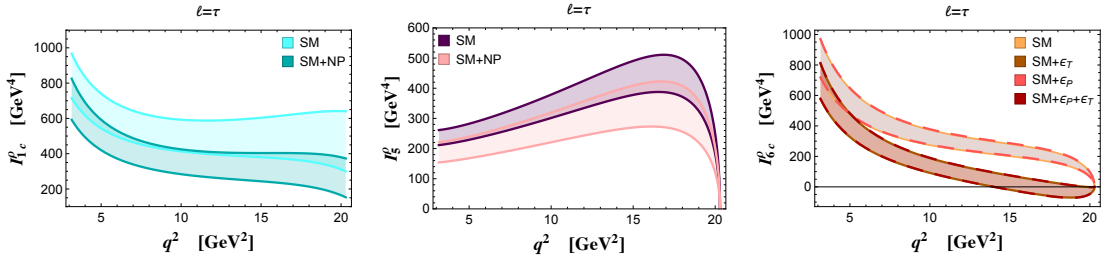

Figure 8. $\bar{B} \to \rho(\pi\pi)\,\tau^-\,\bar{\nu}_\tau$: angular coefficient functions $I_{1c}^\rho(q^2)$ (**left**), $I_5^\rho(q^2)$ (**middle**), $I_{6c}^\rho(q^2)$ (**right**).

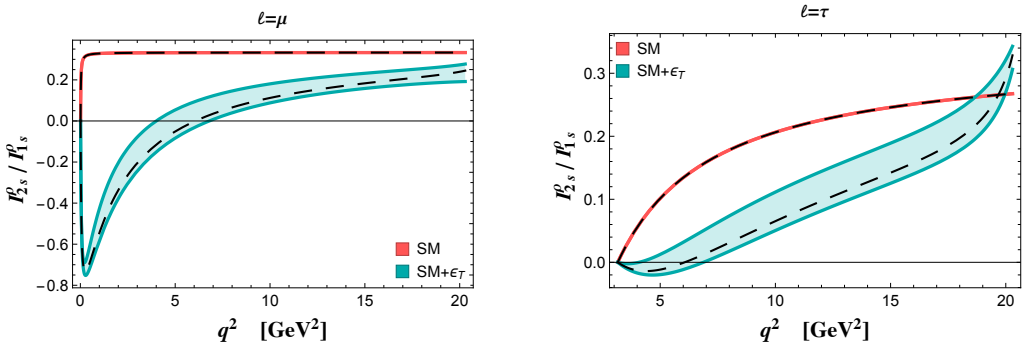

Figure 9. Ratio $R^{\rho}_{2s/1s}$ in (7) for $\bar{B} \to \rho(\pi\pi)\,\mu^-\,\bar{\nu}_\mu$ (**left**) and $\bar{B} \to \rho(\pi\pi)\,\tau^-\,\bar{\nu}_\mu$ (**right**). The dashed lines are the Large Energy result (extrapolated to the full q^2 range).

The function I^{ρ}_{6c}, shown for SM and NP in the right panel of Figure 5, is sensitive to ϵ_V, ϵ_P, ϵ_T. Different possibilities can be envisaged [44]:

(1) If there is no NP ($\epsilon_P = \epsilon_T = 0$), I^{ρ}_{6c} has no zero (right panel of Figure 5).

(2) For NP with $\epsilon_T = 0$ and $\epsilon_P \neq 0$, $(I^{\rho}_{6c})|_{\epsilon_T \simeq 0}$ has a zero at $q^2_0 = -\dfrac{m_b + m_u}{m_\ell}\dfrac{1}{\mathrm{Re}[\epsilon_P]}$, whose measurement would determine $\mathrm{Re}[\epsilon_P]$. We show I^{ρ}_{6c} in the left panel of Figure 10 in the region where the zero is present, and q^2_0 versus $\mathrm{Re}[\epsilon_P]$ in the middle panel of the same figure.

(3) For NP with $\epsilon_P = 0$ and $\epsilon_T \neq 0$, $(I^{\rho}_{6c})|_{\epsilon_P \simeq 0}$ has a zero if $\mathrm{Re}[\epsilon_T] > 0$, its position has a form factor dependence (right panel of Figure 10).

(4) Finally, if there is NP with both $\epsilon_P \neq 0$ and $\epsilon_T \neq 0$, both real and imaginary parts of ϵ_P and ϵ_T are involved, and two zeroes are possible.

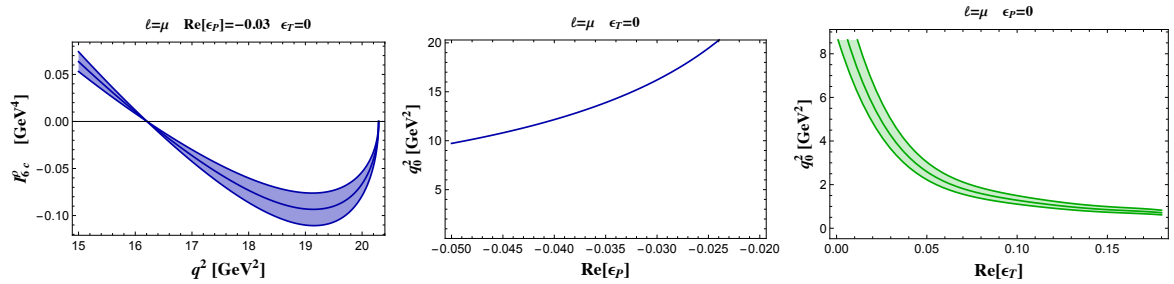

Figure 10. $\bar{B} \to \rho(\pi\pi)\,\mu^-\,\bar{\nu}_\mu$ mode: $I^{\rho}_{6c}(q^2)$ (**left**), and position of the zero q^2_0 varying $\mathrm{Re}(\epsilon_P)$ with $\epsilon_T = 0$ (**middle panel**) and $\mathrm{Re}(\epsilon_T)$ with $\epsilon_P = 0$ (**right**).

Integrating the 4-dimensional distribution several observables can be constructed. The q^2-dependent forward-backward (FB) lepton asymmetry

$$A_{FB}(q^2) = \left[\int_0^1 dcos\,\theta\,\frac{d^2\Gamma}{dq^2 dcos\,\theta} - \int_{-1}^0 dcos\,\theta\,\frac{d^2\Gamma}{dq^2 dcos\,\theta}\right] \Big/ \frac{d\Gamma}{dq^2} \tag{11}$$

is given by

$$A_{FB}(q^2) = \frac{3(I^{\rho}_{6c} + 2I^{\rho}_{6s})}{6I^{\rho}_{1c} + 12I^{\rho}_{1s} - 2I^{\rho}_{2c} - 4I^{\rho}_{2s}}. \tag{12}$$

The transverse forward-backward (TFB) asymmetry, that is, the FB asymmetry for transversely polarized ρ, is given by

$$A^T_{FB}(q^2) = \frac{3I^{\rho}_{6s}}{6I^{\rho}_{1s} - 2I^{\rho}_{2s}}. \tag{13}$$

A_{FB} and A^T_{FB} are shown in Figure 11 for $\ell = \mu$ and $\ell = \tau$. In NP the zero of A_{FB} is shifted in the τ mode. A^T_{FB} is sensitive to the new operators, and in the case of τ it has a zero absent in SM.

There are observables which depend on the ρ polarization, namely the differential branching ratio for longitudinally (L) and transversely (T) polarized ρ, as a function of q^2 or of one of the angles θ, θ_V: $d\mathcal{B}_{L(T)}/dq^2$, $d\mathcal{B}_{L(T)}/dcos\theta$ and $d\mathcal{B}_{L(T)}/dcos\theta_V$. They are shown in Figure 12 for $\ell = \mu$ and $\ell = \tau$.

Integrating the distributions we obtain for the ρ mode: $F_L(\bar{B} \to \rho\mu^-\bar{\nu}_\mu)|_{SM} = 0.52 \pm 0.15$, $\mathcal{B}(\bar{B}^0 \to \rho^+\mu^-\bar{\nu}_\mu)|_{SM} = (3.37 \pm 0.52) \times 10^{-4} \times \left(\frac{|V_{ub}|}{0.0035}\right)^2$, and for the τ mode $F_L(\bar{B} \to \rho\tau^-\bar{\nu}_\tau)|_{SM} = 0.50 \pm 0.13$, $\mathcal{B}(\bar{B}^0 \to \rho^+\tau^-\bar{\nu}_\tau)|_{SM} = (1.80 \pm 0.25) \times 10^{-4} \times \left(\frac{|V_{ub}|}{0.0035}\right)^2$. For $B \to \pi$ we have: $\mathcal{B}(\bar{B}^0 \to \pi^+\mu^-\bar{\nu}_\mu)|_{SM} = (1.5 \pm 0.1) \times 10^{-4} \times \left(\frac{|V_{ub}|}{0.0035}\right)^2$ and $\mathcal{B}(\bar{B}^0 \to \pi^+\tau^-\bar{\nu}_\tau)|_{SM} = (0.92 \pm 0.06) \times 10^{-4} \times \left(\frac{|V_{ub}|}{0.0035}\right)^2$. As shown in Table 1, the ratios

$$R_\pi = \frac{\mathcal{B}(\bar{B} \to \pi\tau^-\bar{\nu}_\tau)}{\mathcal{B}(\bar{B} \to \pi\ell^-\bar{\nu}_\ell)} \quad , \qquad R_\rho = \frac{\mathcal{B}(\bar{B} \to \rho\tau^-\bar{\nu}_\tau)}{\mathcal{B}(\bar{B} \to \rho\ell^-\bar{\nu}_\ell)} \tag{14}$$

are modified by the NP operators in (1). The deviations are correlated, and large effects are possible varying the effective couplings in their allowed ranges (Figure 13).

Table 1. R_π and R_ρ in Equation (14) in SM and in NP at the benchmark point.

	SM	NP (Benchmark Point)
R_π	0.60 ± 0.01	0.75 ± 0.02
R_ρ	0.53 ± 0.02	0.49 ± 0.02

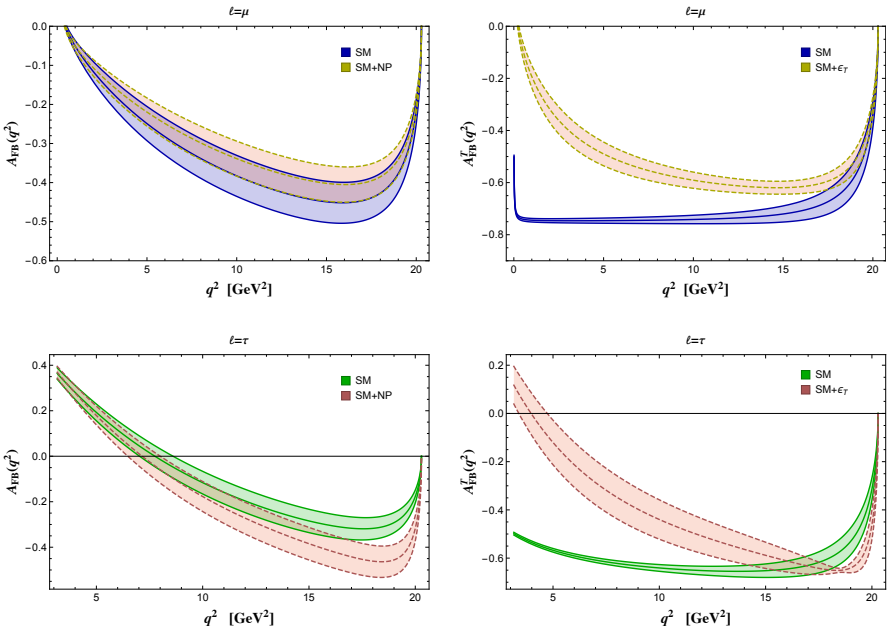

Figure 11. Forward-backward (FB) lepton asymmetries (11) (**left**) and (13) (**right**) for $\bar{B} \to \rho\,\mu^-\,\bar{\nu}_\mu$ (**top line**) and $\bar{B} \to \rho\,\tau^-\,\bar{\nu}_\mu$ (**bottom line**).

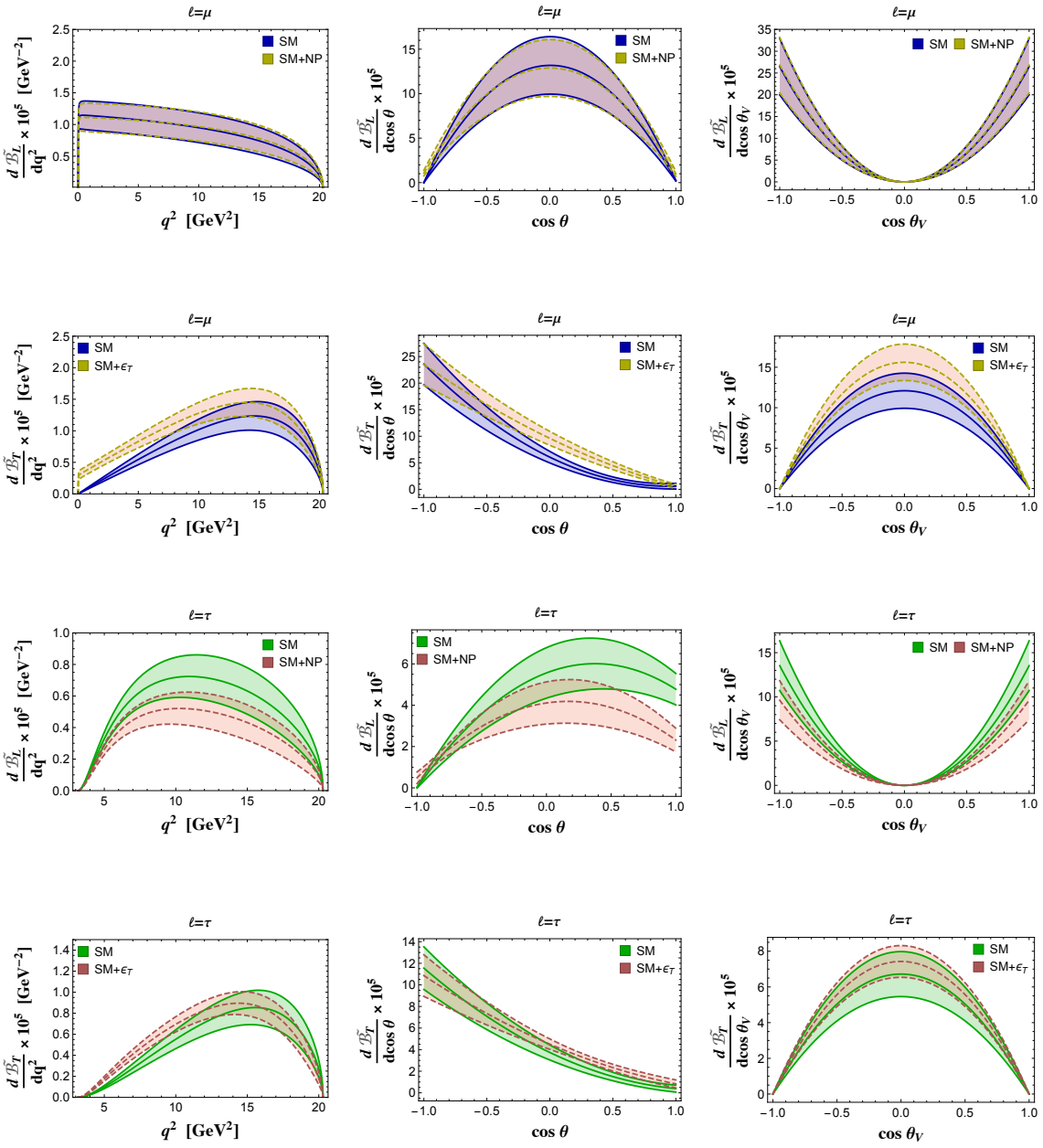

Figure 12. $\bar{B} \to \rho\, \mu^-\, \bar{\nu}_\mu$ mode: distributions $d\tilde{\mathcal{B}}_L/dq^2$, $d\tilde{\mathcal{B}}_L/d\cos\theta$ and $d\tilde{\mathcal{B}}_L/d\cos\theta_V$ (plots in the first row) and $d\tilde{\mathcal{B}}_T/dq^2$, $d\tilde{\mathcal{B}}_T/d\cos\theta$ and $d\tilde{\mathcal{B}}_T/d\cos\theta_V$ (plots in the second row), with $\tilde{\mathcal{B}} = \mathcal{B}/\mathcal{B}(\rho \to \pi\pi)$ for SM and NP. The plots in the third and fourth row are the analogous distributions for $\bar{B} \to \rho\, \tau^-\, \bar{\nu}_\tau$.

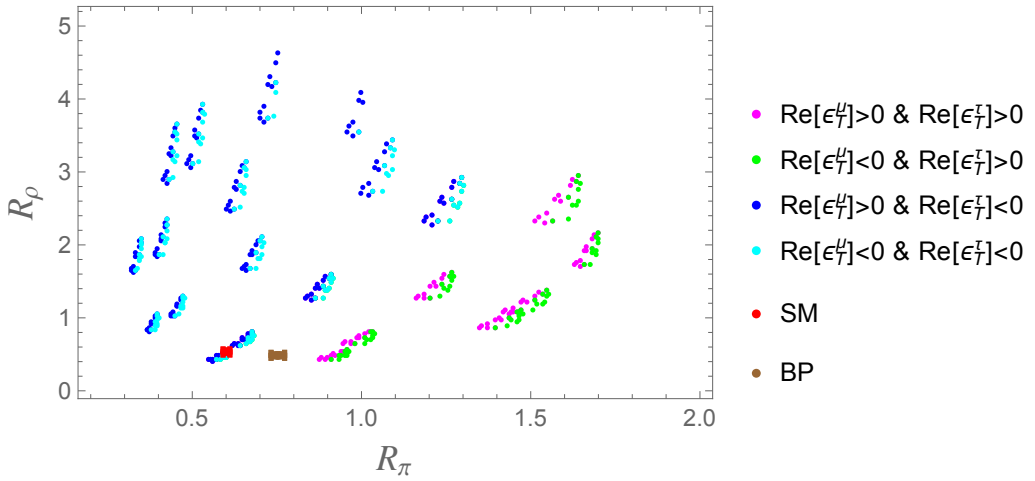

Figure 13. R_ρ vs R_π correlation when only the tensor operator is included in (1). The colors correspond to the different signs of $\mathrm{Re}(\epsilon_T^\mu)$ and $\mathrm{Re}(\epsilon_T^\tau)$ in the range of the parameter space. The red and brown points correspond to SM and NP at the benchmark point.

6. $\bar{B} \to a_1(1260)\ell^-\bar{\nu}_\ell$

We analyze the $\bar{B} \to a_1(\rho\pi)\ell^-\bar{\nu}_\ell$ mode in SM and in the NP extension Equation (1) at the same benchmark points for $\epsilon_{V,S,T}^\ell$. Exclusive hadronic B decays into $a_1(1260)$ have been studied at the B factories considering the dominant $a_1 \to \rho\pi$ mode, and the measurements of the semileptonic $\bar{B} \to a_1$ mode are within the experimental reach, in particular at Belle II. The study of $\bar{B} \to a_1\ell^-\bar{\nu}_\ell$ requires an assessment of the accuracy of the hadronic quantities. We use the set in Reference [60], for which an uncertainty of about 20% is quoted. The angular coefficient functions, for the μ and τ modes and for both the ρ polarizations are in Figures 14 and 15 and in Figures 16 and 17, respectively. In general, the hadronic uncertainties obscure the effect of the NP operators. Nevertheless, there are coefficient functions in which deviations from SM can be observed, namely $I_{2s,\parallel}^{a_1}(q^2)$, $I_{6c,\parallel}^{a_1}(q^2)$ (Figure 14) and $I_{2c,\perp}^{a_1}(q^2)$ (Figure 16) for the μ channel, $I_{1s,\parallel}^{a_1}(q^2)$, $I_{6s,\parallel}^{a_1}(q^2)$ (Figure 15) and $I_{1c\perp}^{a_1}(q^2)$, $I_{6c\perp}^{a_1}(q^2)$ (Figure 16) for the τ mode. The forward/backward lepton asymmetry shows sizable deviations from SM in the case of τ (Figure 18).

For the ratio $R_{a_1} = \dfrac{\mathcal{B}(\bar{B} \to a_1(1260)\tau^-\bar{\nu}_\tau)}{\mathcal{B}(\bar{B} \to a_1(1260)\ell^-\bar{\nu}_\ell)}$ we obtain, in the SM and for NP at the benchmark point,

$$R_{a_1}^{SM} = 0.44 \pm 0.07 \ , \qquad R_{a_1}^{NP} = 0.67 \pm 0.12 \ , \tag{15}$$

with individual branching fractions in SM $\mathcal{B}(\bar{B} \to a_1\,\mu^-\bar{\nu}_\mu) = (3.0 \pm 1.7) \times 10^{-4}$ and $\mathcal{B}(\bar{B} \to a_1\,\tau^-\bar{\nu}_\tau) = (1.3 \pm 0.6) \times 10^{-4}$ [60].

Summarizing the complementarity between the various B modes to the NP search, we remark that the presence of the tensor operator in (1) can be established independently of the other operators, from deviations of the observables that depend only on ϵ_T, for example, those involving transversely polarized ρ and a_1. $|\epsilon_T|$ is constrained looking at the zero of the ratios in Equations (7) and (8). A correlation between the position of the zero in the ρ and a_1 channels should be observed.

If the pseudoscalar operator is present, without other NP structures, deviations should be observed in leptonic B decays and in the semileptonic decay to ρ, not in π and a_1 modes. Determining the position of the zero in I_{6c}^{ρ} would constrain $\mathrm{Re}[\epsilon_P]$. Zeroes should not be present in $I_{6c,\parallel}^{a_1}$. On the other hand, if the scalar operator is present without additional NP structures, deviations should be observed in semileptonic B decays to π and a_1. A zero would be present in $I_{6c,\parallel}^{a_1}$, not in I_{6c}^{ρ}. All operators would manifest in correlated patterns of deviations.

Precise measurements of modes with final τ provide new important tests of LFU. R_ρ and R_π give information on the relative sign of $\mathrm{Re}[\epsilon_T^\mu]$ and $\mathrm{Re}[\epsilon_T^\tau]$. The $a_1(1260)$ channel plays a significant role in the searches.

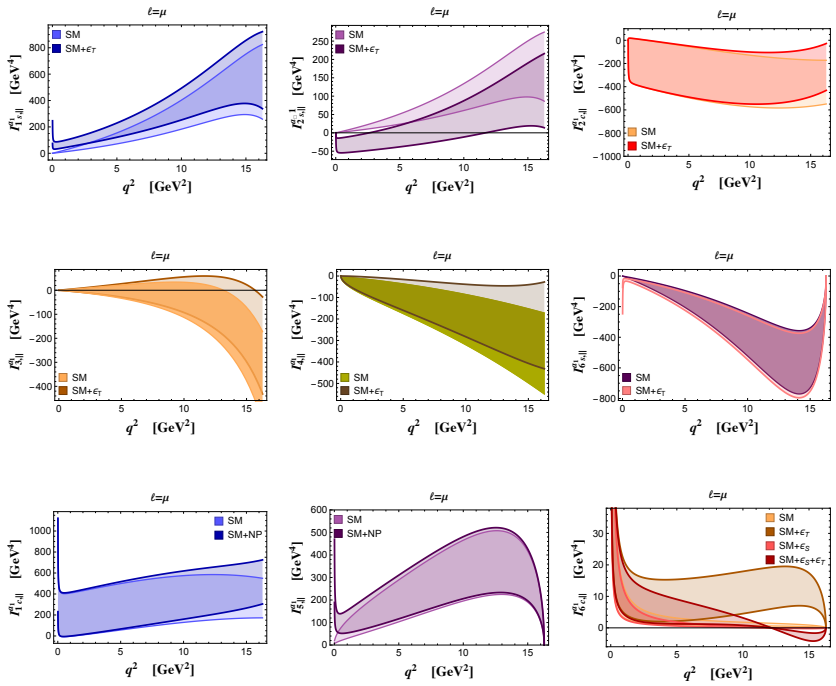

Figure 14. Angular coefficient functions $I_i^{a_1}(q^2)$ in SM and NP (at the benchmark point) for $\bar{B} \to a_1(\rho_\parallel \pi)\, \mu^-\, \bar{\nu}_\mu$ using the form factors in Reference [60]. The band widths for SM and NP, with colors indicated in each plot, are due to the form factor uncertainty.

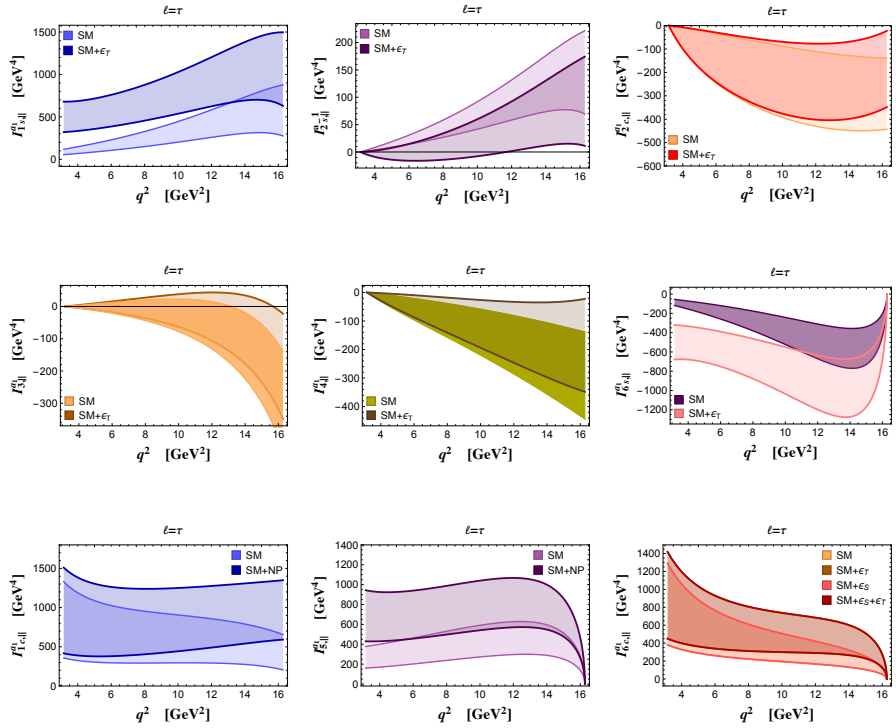

Figure 15. Angular coefficient functions for $\bar{B} \to a_1(\rho_\parallel \pi)\, \tau^-\, \bar{\nu}_\tau$ (same notations as in Figure 14).

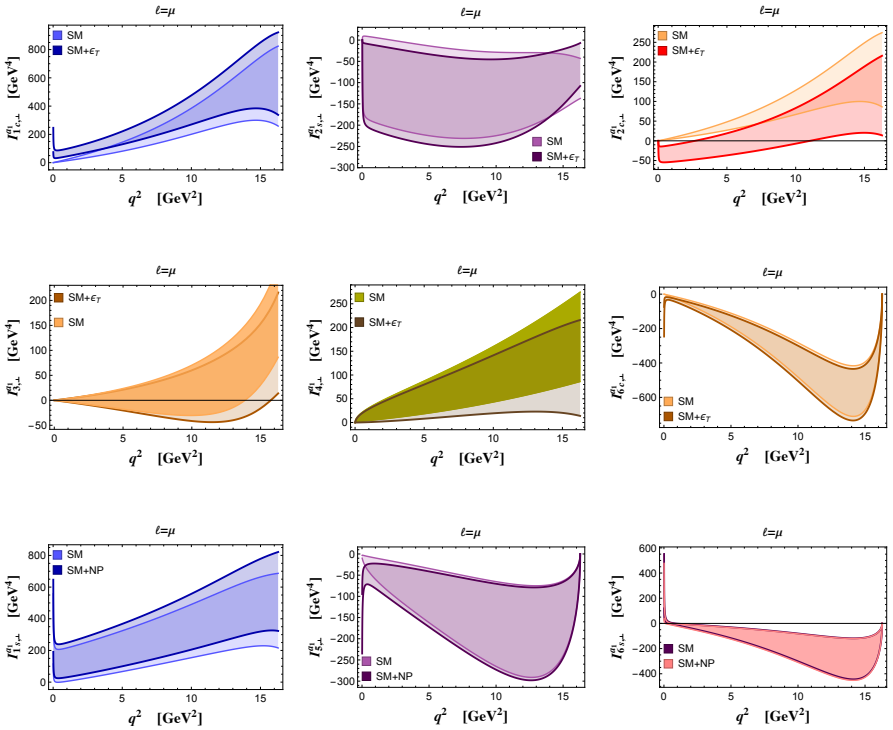

Figure 16. Angular coefficient functions for $\bar{B} \to a_1(\rho_\perp \pi)\, \mu^-\, \bar{\nu}_\mu$ (same notations as in Figure 14).

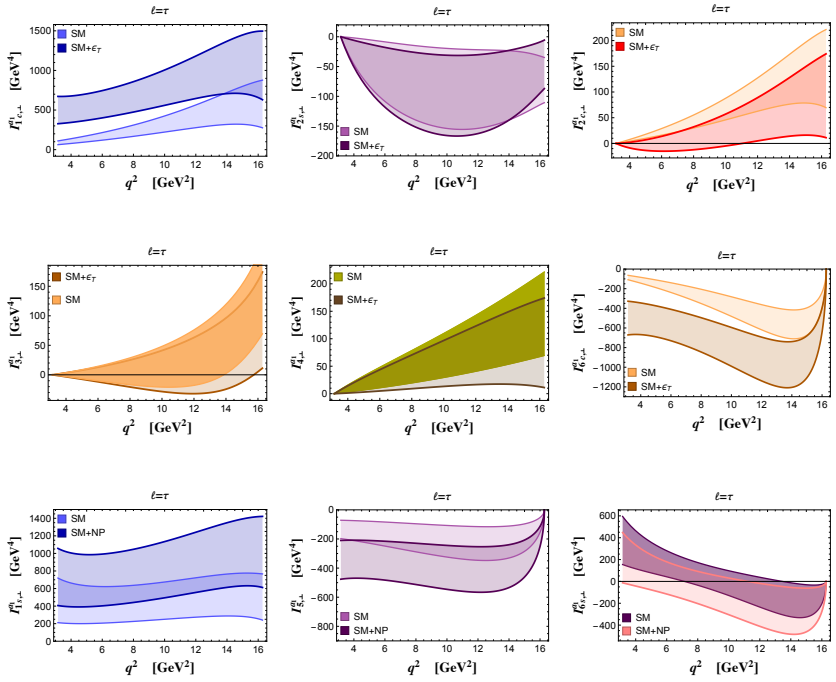

Figure 17. Angular coefficient functions for $\bar{B} \to a_1(\rho_\perp \pi)\, \tau^-\, \bar{\nu}_\tau$ (same notations as in Figure 14).

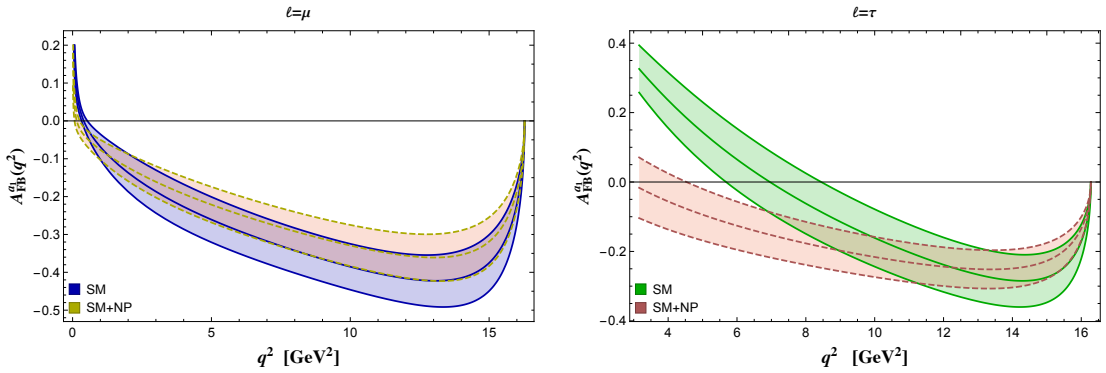

Figure 18. $\bar{B} \to a_1\, \ell^-\, \bar{\nu}_\ell$: FB lepton asymmetries for $\ell = \mu$ (**left**) and τ (**right**).

7. Outlook

The anomalies observed in $b \to c$ semileptonic modes also require new precision analyses of the CKM suppressed $b \to u$ processes. We have discussed the impact of an extended effective $b \to u$ Hamiltonian on purely leptonic B decays, on $\bar{B} \to \pi \ell^- \bar{\nu}_\ell$ and, in details, on $\bar{B} \to \rho(\pi\pi)\ell^- \bar{\nu}_\ell$ and $\bar{B} \to a_1(\rho\pi)\ell^- \bar{\nu}_\ell$, which involve more than one hadron in the final state. For these two modes we have studied the sensitivity of the 4-dimensional angular distributionst to different NP operators. The quantum numbers of the light mesons select the contributions of the NP terms, and complementary information can be gained on the new operators in the effective Hamiltonian. Some observables have zeroes absent in SM. Comparing the modes into μ and τ, LF universality in $b \to u$ weak transitions is probed. The error connected to the hadronic matrix elements represents a sizable uncertainty, in particular for the a_1 mode. The Large Energy Limit, in which the number of hadronic form factors is reduced, is therefore useful for the analyses.

There are exciting perspectives for NP searches in heavy hadron decays in the coming years, in particular investigating $b \to u$ induced semileptonic B modes.

Author Contributions: All authors have equally contributed to this review. All authors have read and agreed to the published version of the manuscript.

Funding: The studies here described have been carried out within the INFN project (Iniziativa Specifica) QFT-HEP.

Acknowledgments: PC thanks Prof. Mikhail A. Ivanov and the other Organizers for invitation to give this lecture at the Helmholtz International Summer School (HISS)—Dubna International Advanced School of Theoretical Physics "Quantum Field Theory at the Limits: from Strong Fields to Heavy Quarks", 2019.

Conflicts of Interest: The authors declare no conflict of interest.

Appendix A. Parametrization of the $B \to \pi$ form Factors

The $B \to \pi$ form factors, in the decomposition of the weak matrix element as given in Reference [44], can be expressed in the form

$$\begin{aligned} f_{+,T}(t) &= \frac{1}{1-\frac{t}{m^2_{B^*}}} \sum_{n=0}^{N-1} a_n \left[z(t)^n - \frac{n}{N}(-1)^{n-N} z(t)^N \right] \\ f_0(t) &= \sum_{n=0}^{N-1} a_n z(t)^n, \end{aligned} \tag{A1}$$

with

$$z(t) = \frac{\sqrt{t_+ - t} - \sqrt{t_+ - t_0}}{\sqrt{t_+ - t} + \sqrt{t_+ - t_0}} \tag{A2}$$

and different parameters a_n for each form factor. In this expression $t_+ = (m_B + m_\pi)^2$, and t_0 is chosen at $t_0 = (m_B + m_\pi)\left(\sqrt{m_B} - \sqrt{m_\pi}\right)^2$. The values for a_n in Table A1 for $f_{+,0,T}$, satisfying the condition $f_+(0) = f_0(0)$, are obtained using Light-Cone QCD sum rule results in the range $m_\ell^2 \leq t \leq 12$ GeV^2 [61,62] and lattice QCD results for 16 GeV$^2 \leq t \leq (m_B - m_\pi)^2$ [63]. Other quantities used in the above analysis are the quark masses $m_u = 2.16^{+0.49}_{-0.26}$ MeV (in the $\overline{MS}$ scheme at $\mu = 2$ GeV) and $\overline{m}_b(\overline{m}_b) = 4.18^{+0.04}_{-0.03}$ GeV [53]. The B^- decay constant is set to $f_B = 188 \pm 7$ MeV [63].

Table A1. Parameters of $B \to \pi$ form factors in Equation (A1).

	$f_+^{B\to\pi}$	$f_0^{B\to\pi}$	$f_T^{B\to\pi}$
a_0	0.416 (20)	0.492 (20)	0.400 (21)
a_1	−0.430	−1.35	−0.50
a_2	0.114	2.50	0.00076
a_3			0.534

References

1. Lees, J.P.; Poireau, V.; Tisserand, V.; Grauges, E.; Palano, A.; Eigen, G.; Stugu, B.; Brown, D.N.; Kerth, L.T.; Kolomensky, Y.G.; et al. Evidence for an excess of $\bar{B} \to D^{(*)}\tau^-\bar{\nu}_\tau$ decays. *Phys. Rev. Lett.* **2012**, *109*, 101802. [CrossRef] [PubMed]
2. Lees, J.P.; Poireau, V.; Tisserand, V.; Grauges, E.; Palano, A.; Eigen, G.; Stugu, B.; Brown, D.N.; Kerth, L.T.; Kolomensky, Y.G.; et al. Measurement of an Excess of $\bar{B} \to D^{(*)}\tau^-\bar{\nu}_\tau$ Decays and Implications for Charged Higgs Bosons. *Phys. Rev.* **2013**, *D88*, 072012.
3. Huschle, M.; Kuhr, T.; Heck, M.; Goldenzweig, P.; Abdesselam, A.; Adachi, I.; Adamczyk, K.; Aihara, H.; Al Said, S.; Arinstein, K.; et al. Measurement of the branching ratio of $\bar{B} \to D^{(*)}\tau^-\bar{\nu}_\tau$ relative to $\bar{B} \to D^{(*)}\ell^-\bar{\nu}_\ell$ decays with hadronic tagging at Belle. *Phys. Rev.* **2015**, *D92*, 072014.
4. Sato, Y.; Iijima, T.; Adamczyk, K.; Aihara, H.; Asner, D.M.; Atmacan, H.; Aushev, T.; Ayad, R.; Aziz, T.; Babu, V.; et al. Measurement of the branching ratio of $\bar{B}^0 \to D^{*+}\tau^-\bar{\nu}_\tau$ relative to $\bar{B}^0 \to D^{*+}\ell^-\bar{\nu}_\ell$ decays with a semileptonic tagging method. *Phys. Rev.* **2016**, *D94*, 072007. [CrossRef]
5. Hirose, S.; Iijima, T.; Adachi, I.; Adamczyk, K.; Aihara, H.; Al Said, S.; Asner, D.M.; Atmacan, H.; Aulchenko, V.; Aushev, T.; et al. Measurement of the τ lepton polarization and $R(D^*)$ in the decay $\bar{B} \to D^*\tau^-\bar{\nu}_\tau$. *Phys. Rev. Lett.* **2017**, *118*, 211801. [CrossRef]
6. Hirose, S.; Iijima, T.; Adachi, I.; Adamczyk, K.; Aihara, H.; Al Said, S.; Asner, D.M.; Atmacan, H.; Aulchenko, V.; Aushev, T.; et al. Measurement of the τ lepton polarization and $R(D^*)$ in the decay $\bar{B} \to D^*\tau^-\bar{\nu}_\tau$ with one-prong hadronic τ decays at Belle. *Phys. Rev.* **2018**, *D97*, 012004. [CrossRef]
7. Aaij, R.; Adeva, B.; Adinolfi, M.; Affolder, A.; Ajaltouni, Z.; Akar, S.; Albrecht, J.; Alessio, F.; Alexander, M.; Ali, S.; et al. Measurement of the ratio of branching fractions $\mathcal{B}(\bar{B}^0 \to D^{*+}\tau^-\bar{\nu}_\tau)/\mathcal{B}(\bar{B}^0 \to D^{*+}\mu^-\bar{\nu}_\mu)$. *Phys. Rev. Lett.* **2015**, *115*, 111803. [CrossRef]
8. Aaij, R.; Adeva, B.; Adinolfi, M.; Ajaltouni, Z.; Akar, S.; Albrecht, J.; Alessio, F.; Alexander, M.; Albero, A.A.; Ali, S.; et al. Test of Lepton Flavor Universality by the measurement of the $B^0 \to D^{*-}\tau^+\nu_\tau$ branching fraction using three-prong τ decays. *Phys. Rev.* **2018**, *D97*, 072013. [CrossRef]
9. Aaij, R.; Adeva, B.; Adinolfi, M.; Ajaltouni, Z.; Akar, S.; Albrecht, J.; Alessio, F.; Alexander, M.; Albero, A.A.; Ali, S.; et al. Measurement of the ratio of the $B^0 \to D^{*-}\tau^+\nu_\tau$ and $B^0 \to D^{*-}\mu^+\nu_\mu$ branching fractions using three-prong τ-lepton decays. *Phys. Rev. Lett.* **2018**, *120*, 171802. [CrossRef]
10. Amhis, Y.; Banerjee, S.; Ben-Haim, E.; Bernlochner, F.; Bozek, A.; Bozzi, C.; Chrząszcz, M.; Dingfelder, J.; Duell, S.; Gersabeck, M.; et al. Averages of b-hadron, c-hadron, and τ-lepton properties as of summer 2016. *Eur. Phys. J.* **2017**, *C77*, 895.
11. Fajfer, S.; Kamenik, J.F.; Nisandzic, I. On the $B \to D^*\tau\bar{\nu}_\tau$ Sensitivity to New Physics. *Phys. Rev.* **2012**, *D85*, 094025.
12. Biancofiore, P.; Colangelo, P.; De Fazio, F. On the anomalous enhancement observed in $B \to D^{(*)}\tau\bar{\nu}_\tau$ decays. *Phys. Rev.* **2013**, *D87*, 074010.

13. Aaij, R.; Adeva, B.; Adinolfi, M.; Ajaltouni, Z.; Akar, S.; Albrecht, J.; Alessio, F.; Alexander, M.; Albero, A.A.; Ali, S.; et al. Measurement of the ratio of branching fractions $\mathcal{B}(B_c^+ \to J/\psi\tau^+\nu_\tau)/\mathcal{B}(B_c^+ \to J/\psi\mu^+\nu_\mu)$. *Phys. Rev. Lett.* **2018**, *120*, 121801. [CrossRef] [PubMed]
14. Dutta, R.; Bhol, A. $B_c \to (J/\psi, \eta_c)\tau\nu$ semileptonic decays within the standard model and beyond. *Phys. Rev.* **2017**, *D96*, 076001.
15. Watanabe, R. New Physics effect on $B_c \to J/\psi\tau\bar{\nu}$ in relation to the $R_{D^{(*)}}$ anomaly. *Phys. Lett.* **2018**, *B776*, 5. [CrossRef]
16. Tran, C.T.; Ivanov, M.A.; Koerner, J.G.; Santorelli, P. Implications of new physics in the decays $B_c \to (J/\psi, \eta_c)\tau\nu$. *Phys. Rev.* **2018**, *D97*, 054014. [CrossRef]
17. Leljak, D.; Melic, B.; Patra, M. On lepton flavour universality in semileptonic $B_c \to \eta_c$, J/ψ decays. *JHEP* **2019**, *5*, 094.
18. Aaij, R.; Adeva, B.; Adinolfi, M.; Ajaltouni, Z.; Akar, S.; Albrecht, J.; Alessio, F.; Alexander, M.; Albero, A.A.; Ali, S.; et al. Search for lepton-universality violation in $B^+ \to K^+\ell^+\ell^-$ decays. *Phys. Rev. Lett.* **2019**, *122*, 191801.
19. Aaij, R.; Adeva, B.; Adinolfi, M.; Ajaltouni, Z.; Akar, S.; Albrecht, J.; Alessio, F.; Alexander, M.; Albero, A.A.; Ali, S.; et al. Test of lepton universality with $B^0 \to K^{*0}\ell^+\ell^-$ decays. *JHEP* **2017**, *8*, 055.
20. Abdesselam, A.; Adachi I.; Adamczyk, K.; Aihara, H.; Al Said, S.; Arinstein, K.; Arita, Y.; Asner, D.M.; Atmacan, H.; Ahn, J.K.; et al. Test of lepton flavor universality in $B \to K^*\ell^+\ell^-$ decays at Belle. *arXiv* **2019**, arXiv:hep-ex/1904.02440.
21. Aaij, R.; Adeva, B.; Adinolfi, M.; Ajaltouni, Z.; Akar, S.; Albrecht, J.; Alessio, F.; Alexander, M.; Albero, A.A.; Ali, S.; et al. Test of lepton universality with $\Lambda_b^0 \to pK^-\ell^+\ell^-$ decays. *arXiv* **2019**, arXiv:hep-ex/1912.08139.
22. Bifani, S.; Descotes-Genon, S.; Romero Vidal, A.; Schune, M.H. Review of Lepton Universality tests in B decays. *J. Phys.* **2019**, *G46*, 023001. [CrossRef]
23. Lees, J.P.; Poireau, V.; Tisserand, V.; Grauges, E.; Palano, A.; Eigen, G.; Stugu, B.; Brown, D.N.; Kerth, L.T.; Kolomensky, Y.G.; et al. A test of heavy quark effective theory using a four-dimensional angular analysis of $\overline{B} \to D^*\ell^-\overline{\nu}_\ell$. *arXiv* **2019**, arXiv:hep-ex/1903.10002.
24. Waheed, E.; Urquijo, P.; Ferlewicz, D.; Adachi, I.; Adamczyk, K.; Ahn, J.K.; Aihara, H.; Al Said, S.; Arinstein, K.; Arita, Y.; et al. Measurement of CKM Matrix Element $|V_{cb}|$ from $\bar{B} \to D^{*+}\ell^-\bar{\nu}_\ell$. *arXiv* **2018**. arXiv:hep-ex/1809.03290.
25. Aaij, R.; Adeva, B.; Adinolfi, M.; Ajaltouni, Z.; Akar, S.; Albrecht, J.; Alessio, F.; Alexander, M.; Albero, A.A.; Ali, S.; et al. Measurement of $|V_{cb}|$ with $B_s^0 \to D_s^{(*)-}\mu^+\nu_\mu$ decays. *arXiv* **2020**, arXiv:hep-ex/2001.03225.
26. Jaiswal, S.; Nandi, S.; Patra, S.K. Extraction of $|V_{cb}|$ from $B \to D^{(*)}\ell\nu_\ell$ and the Standard Model predictions of $R(D^{(*)})$. *JHEP* **2017**, *12*, 060. [CrossRef]
27. Bigi, D.; Gambino, P.; Schacht, S. A fresh look at the determination of $|V_{cb}|$ from $B \to D^*\ell\nu$. *Phys. Lett.* **2017**, *B769*, 441. [CrossRef]
28. Grinstein, B.; Kobach, A. Model-Independent Extraction of $|V_{cb}|$ from $\bar{B} \to D^*\ell\overline{\nu}$. *Phys. Lett.* **2017**, *B771*, 359. [CrossRef]
29. Gambino, P.; Jung, M.; Schacht, S. The V_{cb} puzzle: An update. *Phys. Lett.* **2019**, *B795*, 386–390. [CrossRef]
30. Colangelo, P.; De Fazio, F. Tension in the inclusive versus exclusive determinations of $|V_{cb}|$: A possible role of new physics. *Phys. Rev.* **2017**, *D95*, 011701. [CrossRef]
31. Alonso, R.; Kobach, A.; Martin Camalich, J. New physics in the kinematic distributions of $\bar{B} \to D^{(*)}\tau^-(\to \ell^-\bar{\nu}_\ell\nu_\tau)\bar{\nu}_\tau$. *Phys. Rev.* **2016**, *D94*, 094021. [CrossRef]
32. Ligeti, Z.; Papucci, M.; Robinson, D.J. New Physics in the Visible Final States of $B \to D^{(*)}\tau\nu$. *JHEP* **2017**, *1*, 083. [CrossRef]
33. Alok, A.K.; Kumar, D.; Kumbhakar, S.; Sankar, S.U. D^* polarization as a probe to discriminate new physics in $\bar{B} \to D^*\tau\bar{\nu}$. *Phys. Rev.* **2017**, *D95*, 115038. [CrossRef]
34. Colangelo, P.; De Fazio, F. Scrutinizing $\overline{B} \to D^*\,(D\pi)\,\ell^-\overline{\nu}_\ell$ and $\overline{B} \to D^*\,(D\gamma)\,\ell^-\overline{\nu}_\ell$ in search of new physics footprints. *JHEP* **2018**, *6*, 082. [CrossRef]
35. Becirevic, D.; Fedele, M.; Nisandzic, I.; Tayduganov, A. Lepton Flavor Universality tests through angular observables of $\overline{B} \to D^{(*)}\ell\overline{\nu}$ decay modes. *arXiv* **2019**, arXiv:hep-ph/1907.02257.
36. Chen, C.H.; Nam, S.H. Left-right mixing on leptonic and semileptonic $b \to u$ decays. *Phys. Lett.* **2008**, *B666*, 462–466. [CrossRef]

37. Buras, A.J.; Gemmler, K.; Isidori, G. Quark flavour mixing with right-handed currents: an effective theory approach. *Nucl. Phys.* **2011**, *B843*, 107. [CrossRef]
38. Crivellin, A. Effects of right-handed charged currents on the determinations of $|V(ub)|$ and $|V(cb)|$. *Phys. Rev.* **2010**, *D81*, 031301.
39. Crivellin, A.; Pokorski, S. Can the differences in the determinations of V_{ub} and V_{cb} be explained by New Physics? *Phys. Rev. Lett.* **2015**, *114*, 011802. [CrossRef]
40. Bernlochner, F.U.; Ligeti, Z.; Turczyk, S. New ways to search for right-handed current in B$\to \rho\ell\bar{\nu}$ decay. *Phys. Rev.* **2014**, *D90*, 094003. [CrossRef]
41. Bernlochner, F.U. $B \to \pi\tau\bar{\nu}_\tau$ decay in the context of type II 2HDM. *Phys. Rev.* **2015**, *D92*, 115019.
42. Blanke, M.; Crivellin, A.; Kitahara, T.; Moscati, M.; Nierste, U.; Nisandzic, I. Addendum: "Impact of polarization observables and $B_c \to \tau\nu$ on new physics explanations of the $b \to c\tau\nu$ anomaly". *arXiv* **2019**, arXiv:hep-ph/1905.08253.
43. Banelli, G.; Fleischer, R.; Jaarsma, R.; Tetlalmatzi-Xolocotzi, G. Decoding (Pseudo)-Scalar Operators in Leptonic and Semileptonic *B* Decays. *Eur. Phys. J.* **2018**, *C78*, 911. [CrossRef] [PubMed]
44. Colangelo, P.; De Fazio, F.; Loparco, F. Probing New Physics with $\bar{B} \to \rho(770)\,\ell^-\bar{\nu}_\ell$ and $\bar{B} \to a_1(1260)\,\ell^-\bar{\nu}_\ell$. *Phys. Rev.* **2019**, *D100*, 075037. doi:10.1103/PhysRevD.100.075037 . [CrossRef]
45. Buchmuller, W.; Wyler, D. Effective Lagrangian Analysis of New Interactions and Flavor Conservation. *Nucl. Phys.* **1986**, *B268*, 621. [CrossRef]
46. Cirigliano, V.; Jenkins, J.; Gonzalez-Alonso, M. Semileptonic decays of light quarks beyond the Standard Model. *Nucl. Phys.* **2010**, *B830*, 95. [CrossRef]
47. Jung, M.; Straub, D.M. Constraining new physics in $b \to c\ell\nu$ transitions. *JHEP* **2019**, *1*, 009. [CrossRef]
48. Celis, A.; Jung, M.; Li, X.Q.; Pich, A. Scalar contributions to $b \to c(u)\tau\nu$ transitions. *Phys. Lett.* **2017**, *B771*, 168. [CrossRef]
49. Leljak, D.; Melic, B. $|V_{ub}|$ determination and testing of lepton flavour universality in semileptonic $B_c \to D^{(*)}$ decays. *arXiv* **2019**, arXiv:hep-ph/1909.01213.
50. Aaij, R.; Adeva, B.; Adinolfi, M.; Ajaltouni, Z.; Akar, S.; Albrecht, J.; Alessio, F.; Alexander, M.; Albero, A.A.; Ali, S.; et al. Determination of the quark coupling strength $|V_{ub}|$ using baryonic decays. *Nat. Phys.* **2015**, *11*, 743–747.
51. Charles, J.; Le Yaouanc, A.; Oliver, L.; Pene, O.; Raynal, J.C. Heavy to light form-factors in the heavy mass to large energy limit of QCD. *Phys. Rev.* **1999**, *D60*, 014001.
52. Beneke, M.; Feldmann, T. Symmetry breaking corrections to heavy to light B meson form-factors at large recoil. *Nucl. Phys.* **2001**, *B592*, 3. [CrossRef]
53. Tanabashi, M.; Hagiwara, K.; Hikasa, K.; Nakamura, K.; Sumino, Y.; Takahashi, F.; Tanaka, J.; Agashe, K.; Aielli, G.; Amsler, C. Review of Particle Physics. *Phys. Rev.* **2018**, *D98*, 030001. [CrossRef]
54. Sibidanov, A.; Varvell, K.E.; Adachi, I.; Aihara, H.; Al Said, S.; Asner, D.M.; Aushev, T.; Ayad, R.; Babu, V.; Badhrees, I.; et al. Search for $B^- \to \mu^-\bar{\nu}_\mu$ Decays at the Belle Experiment. *Phys. Rev. Lett.* **2018**, *121*, 031801. [CrossRef] [PubMed]
55. Hamer, P.; Frey, A.; Abdesselam, A.; Adachi, I.; Aihara, H.; Al Said, S.; Arinstein, K.; Asner, D.M.; Aushev, T.; Ayad, R.; et al.; Search for $B^0 \to \pi^-\tau^+\nu_\tau$ with hadronic tagging at Belle. *Phys. Rev.* **2016**, *D93*, 032007.
56. Bharucha, A.; Straub, D.M.; Zwicky, R. $B \to V\ell^+\ell^-$ in the Standard Model from light-cone sum rules. *JHEP* **2016**, *8*, 098. [CrossRef]
57. Ha, H.; Won, E.; Adachi, I.; Aihara, H.; Aziz, T.; Bakich, A.M.; Balagura, V.; Barberio, E.; Bay, A.; Belous, K.; et al. Measurement of the decay $B^0 \to \pi^-\ell^+\nu$ and determination of $|V_{ub}|$. *Phys. Rev.* **2011**, *D83*, 071101.
58. del Amo Sanchez, P.; Lees, J.P.; Poireau, V.; Prencipe, E.; Tisserand, V.; Garra Tico, J.; Grauges, E.; Martinelli, M.; Milanes, D.A.; Palano, A.; et al. Measurement of the $B^0 \to \pi^\ell\ell^+\nu$ and $B^+ \to \eta^{(\prime)}\ell^+\nu$ Branching Fractions, the $B^0 \to \pi^-\ell^+\nu$ and $B^+ \to \eta\ell^+\nu$ Form-Factor Shapes, and Determination of $|V_{ub}|$. *Phys. Rev.* **2011**, *D83*, 052011.
59. Lees, J.P.; Poireau, V.; Tisserand, V.; Grauges, E.; Palano, A.; Eigen, G.; Stugu, B.; Brown, D.N.; Kerth, L.T.; Kolomensky, Y.G.; et al. Branching fraction and form-factor shape measurements of exclusive charmless semileptonic B decays, and determination of $|V_{ub}|$. *Phys. Rev.* **2012**, *D86*, 092004.
60. Li, R.H.; Lu, C.D.; Wang, W. Transition form factors of B decays into p-wave axial-vector mesons in the perturbative QCD approach. *Phys. Rev.* **2009**, *D79*, 034014.

61. Sentitemsu Imsong, I.; Khodjamirian, A.; Mannel, T.; van Dyk, D. Extrapolation and unitarity bounds for the $B \to \pi$ form factor. *JHEP* **2015**, *2*, 126. [CrossRef]
62. Khodjamirian, A.; Rusov, A.V. $B_s \to K\ell\nu_\ell$ and $B_{(s)} \to \pi(K)\ell^+\ell^-$ decays at large recoil and CKM matrix elements. *JHEP* **2017**, *8*, 112. [CrossRef]
63. Aoki, S.; Aoki, Y.; Becirevic, D.; Blum, T.; Colangelo, G.; Collins, S.; Morte, M.D.; Dimopoulos, P.; Dürr, S.; Fukaya, H.; et al. FLAG Review 2019. *arXiv* **2019**, arXiv:hep-lat/1902.08191.